

Draft: THz from ZGP

Broadband terahertz pulse emission from ZnGeP₂

J. D. Rowley,¹ J. K. Pierce,¹ A. T. Brant,¹ L. E. Halliburton,¹ N. C. Giles,²
P. G. Schunemann,³ and A. D. Bristow^{1, a)}

¹⁾*Department of Physics, West Virginia University, Morgantown WV 26506-6315, USA*

²⁾*Department of Engineering Physics, Air Force Institute of Technology, Wright-Patterson Air Force Base, Ohio 45433, USA*

³⁾*BAE Systems, Nashua, New Hampshire 03061, USA*

(Dated: 15 May 2022)

Optical rectification is demonstrated in birefringent (110)-cut ZnGeP₂ (ZGP) providing broadband terahertz (THz) generation. The source is compared to both GaP and GaAs over a wavelength range of 1150 nm to 1600 nm and peak intensities range of 0.5 GW/cm² to 40 GW/cm². ZGP peak-to-peak field amplitude is larger than in the other materials due to either lower nonlinear absorption or an increase second order nonlinearity. This material is well suited to broadband THz generation across a wide range of infrared excitation wavelengths.

PACS numbers: 42.65.-k, 42.65.Ky, 42.70.Nq

^{a)}Electronic mail: alan.bristow@mail.wvu.edu

Over the last decade, broadband sources of intense THz pulses have received significant attention due to the possibility of accessing a diverse range of light-matter interactions and the potential for creating high-speed electronics. For a recent review of the progress see Ulbricht *et. al.*¹ and references therein. Large-area zincblende ($\bar{4}3m$) crystals are commonly used in time-domain terahertz spectroscopy as source and electro-optic (EO) samplers,² due to large second-order nonlinear coefficients. Common issues with materials like GaAs and ZnTe is the optimum wavelength for THz and optical velocity matching is poorly positioned with respect to the onset of nonlinear absorption.

Here we generate broadband THz pulses in ZnGeP₂, a chalcopyrite (pnictide) crystal with $\bar{4}2m$ symmetry, by optical rectification. Optical rectification is a second-order nonlinear optical process that generates a transient D.C. polarization, which typically creates THz radiation for short excitation pulses. Previously, ZnGeP₂ has only been used as a source of narrow-band THz radiation through parametric down conversion^{3,4} and excitation of coherent phonons.⁵ This work verifies that ZGP has a suitable coherence length, high laser-damage thresholds³ and nonlinear figure-of-merit⁶ for this task. ZGP's generation efficiency surpasses that of high-quality and high-resistivity wafers of GaAs and GaP across the infrared, including throughout the datacoms C-band at 1550 nm. This study complements the recent resurgence of interest in ZGP as a nonlinear material, which is driven by high-quality growth.^{7,8}

Undoped ZGP single crystals were grown by horizontal gradient freeze technique.⁷ Samples are $\sim 1\text{-cm}^2$ chips that were cut in the (110) plane and double-side polished for optical transmission measurements. Sample thicknesses are 0.33 mm and 0.93 mm for the short and long crystals respectively. The orientation of the cut crystals was verified by electron paramagnetic resonance (EPR), ensuring that the c-axis is in the plane of the plate. EPR measures the phosphorus hyperfine signal associated with the zinc-vacancy acceptor in as-grown ZGP, differentiating the $\langle 100 \rangle$ and $\langle 001 \rangle$ directions.⁹ ZGP is birefringent due to $\sim 2\%$ lattice compression in the z-axis, which may complicate the THz generation. Non-birefringent reference crystals are undoped, high resistivity (110)-cut GaP (0.13 mm) and GaAs (0.5 mm). Each measurement was performed at normal incidence with the crystal rotated in the plane to optimize the THz signal. A study of the polarization-dependent THz generation is not shown in this letter.

Figure 1(a) shows the time-domain THz-emission spectroscopy setup, which uses 100-fs

pulses from a 1 KHz regenerative laser amplifier. “Signal” pulses from an optical parametric amplifier (OPA) impinge the test nonlinear crystals (NLC), generating THz radiation that is detected by EO sampling. The gate pulse is centered at 800 nm, and the detection sensitivity is $\sim 1 \times 10^{-8} / \sqrt{Hz}$, using a Soleil-Babinet compensator (SBC), Wollaston prism (WP) and balanced (A-B) biased-photodiodes operating close to the shot-noise limit. The excitation pulses are mechanically chopped (C) for phase-sensitive detection and are tunable from 1150 nm to 1600 nm. A long-pass polyvinyl chloride filter (F) prevents the pump light from reaching the EO sampler (ZnTe, 0.1-mm thick).

Figure 1(b) shows a typical THz transient mapped out by the gate pulse when scanning the relative time delay (delay stage, DS). The EO signal is linearly proportional to the THz field $|E_{THz}|$ and the signal yields >100 signal-to-noise ratio. The data reveals a main THz transient and an echo at 12 ps. Additional, oscillations are due to the 3-THz bandwidth of the ZnTe sampling crystal and water absorption, even with a nitrogen purge of the setup. Normalized power spectra were obtained by a fast Fourier transform with a 3-ps window function in analysis; see the inset of the figure. As expected, the spectrum is broadband (~ 0.1 THz to ~ 3 THz). By comparison the spectrum of GaAs peaks at lower frequencies, suggesting that the peak-to-peak electric field strength will be smaller than that obtained from ZGP.¹⁰

Figure 2 shows the peak-intensity dependence of the THz amplitude $|E_{THz}|$ for the 0.33-mm ZGP, 0.13-mm GaP and 0.5-mm GaAs samples, pumped at (a) 1260 nm and (b) 1536 nm. $|E_{THz}|$ is measured as the peak-to-peak voltage change during the main transient, as indicated in Fig. 1(b). Peak-intensity values are corrected to account for reflection losses at the input interface. At low intensities $|E_{THz}|$ increases linearly because $dE_{THz}/dz \propto d_{36}I(z)$, where d_{36} is the nonlinear tensor element. The effective coefficient d_{eff} and d_{36} are interchangeable in the proportionality because all crystals are identically cut. At higher intensities the signal saturates due to nonlinear absorption of the excitation pulse, which follows a generalized form of Beer’s law: $dI(z)/dz = -\alpha I(z) - \beta I^2(z) - \gamma I^3(z) + \dots$, where α is the linear absorption coefficient that is measured in an auxiliary measurement, and β , γ are the two- (2PA), three-photon (3PA) absorption coefficients. Values used to fit the experimental data are shown in Table I. For GaAs the absorption is dominated by 2PA, whereas for the other crystals 3PA dominates. Even neglecting free-carrier absorption by the THz, the fitting parameters are generally in good agreement with values in the

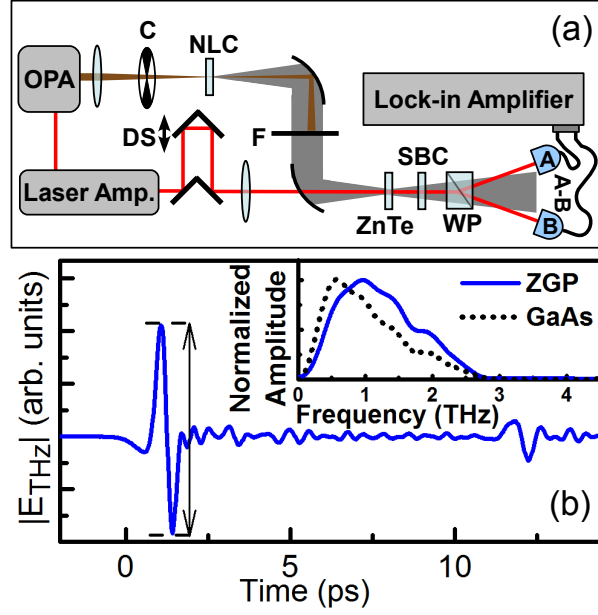


FIG. 1. (color online) (a) Time-domain terahertz (THz) emission spectroscopy setup. (b) Typical THz transient for ZnGeP₂ (ZGP) pumped at 1300 nm. Inset shows normalized power spectra for ZGP and GaAs.

TABLE I. Optical properties of the various semiconductors crystal at 1240(1536) nm, where \times means the term is neglected in the fitting the intensity dependence.

	d_{36} (pm/V)	α (cm ⁻¹)	β (cm/GW)	γ (cm ³ /GW ²)
GaAs	130(119)	1	35	\times
ZGP	70	1.8	\times	0.09(0.11)
GaP	50(45)	3.5	\times	0.08(0.10)

literature.^{11–14}

The difference in crystal length for the relative peak-to-peak $|E_{THz}|$ presented in Fig. 2(a) and (b) skews the results in favor of the longer crystal. Consequently, an estimate of the respective curve shapes and strengths are given in Fig. 2(c) and (d) for the same excitation conditions, but where each crystal is taken to be 0.5 mm thick. After compensating for crystal length, the ZGP still out performs both GaAs and GaP at the wavelengths shown. Small discrepancies in scaling the data for length may arise due to velocity matching at

the two excitation wavelengths. Nonetheless, the trend of ZGP's higher performance is also observed at 1342 nm and 1442 nm (data not shown).

Figure 3 (a) shows the photon energy (wavelength) dependence of the relative peak-to-peak $|E_{THz}|$ from ZGP of two thicknesses, GaP and GaAs. The above intensity dependence is used to normalize the data at each wavelength, account for variations in the OPA emission and the transmission losses through the optical excitation setup. Average pump intensity of $\sim 8 \text{ GW/cm}^2$ was used to minimize the effects of 2PA and 3PA. Consequently, variations in $|E_{THz}|$ due to differences in the nonlinear absorption can be neglected, but effects of crystal thickness or velocity matching cannot. The short ZGP and GaP samples are mostly unaffected by photon energy, showing a flat response. However, the longer ZGP and GaAs data appear to decrease at lower photon energies, and the ZGP response peaks at 1200 nm. The latter result suggests that the long ZGP is affected by a mismatch in the THz and pump pulse velocities.

The velocity matching is quantified by the coherence length $l_c \equiv c/(2\nu_{THz}|n_{THz} - n_g|)$, where c is the speed of light, ν_{THz} and n_{THz} are the phase frequency and refractive index of the THz, and $n_g = n - \lambda \partial n / \partial \lambda$ is the optical group index for the pump pulse with cen-

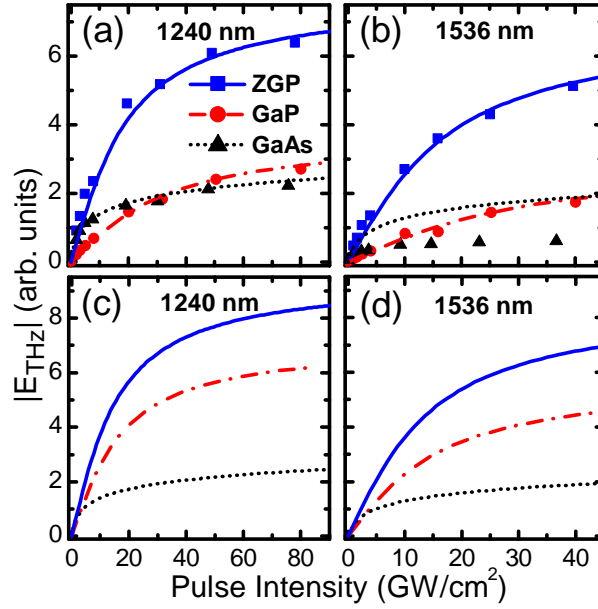


FIG. 2. (color online) Intensity-dependent peak-to-peak THz amplitude for ZGP (0.33 mm), GaP (0.13 mm) and GaAs (0.5 mm) at (a) 1240 nm and (b) 1536 nm. Estimated THz amplitude adjusting for the crystal length, based on a thickness of 0.5 mm for (c) 1240 nm and (d) 1536 nm.

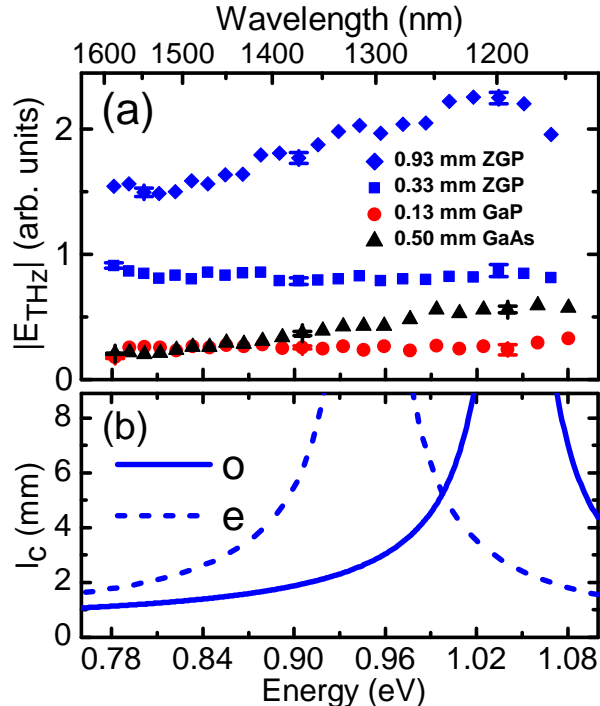


FIG. 3. (color online) (a) Photon energy and wavelength dependence of the peak-to-peak THz amplitude for ZGP, GaP and GaAs. (b) Simulation of the wavelength-dependent coherence length of ZGP for ordinary and extra-ordinary polarization.

tral wavelength λ and corresponding linear refractive index n . Since ZGP is a birefringent crystal the coherence length can be plotted for both ordinary (o) and extra-ordinary (e) polarizations. Figure 3(b) shows the o- and e-ray coherence lengths for ZGP using published dispersions relations^{15,16} and a phase velocity at the peak of the spectrum (1 THz). Comparison of the coherence length to the wavelength-dependence of the long ZGP indicates that velocity matching may indeed be the cause of the peak at 1200 nm. Differences between the peak in $|E_{THz}(\lambda)|$ and $l_c(\lambda)$ are most likely due to inaccuracies in the known values of n_{THz} .

Moderate length ZGP crystals (<1 mm) appear to be efficient THz sources across the infrared because of convenient velocity matching. Therefore, ZGP offers a better alternative than GaAs excited in the telecoms/datacoms window,¹⁷ due to lower multiphoton absorption. It may also operate more efficiently than GaP excited at its optimum coherence length,¹⁸ due to larger d_{eff} and comparable β and γ .⁶

In summary, it has been shown experimentally that ZnGeP_2 is capable of effectively producing broadband THz pulses by optical rectification and that crystal quality and the

birefringence are not impediments to the generation process. While neither the source nor the setup in this study are optimized to compare directly with large-area optical rectification, tilted wave-front, or air-plasma THz sources,¹⁰ the observed response encourages further exploration of THz generation in chalcopyrite crystals by optical rectification.

JDR wishes to thank the WVNano Initiative for support. Research at West Virginia University was funded by the Eberly College of Arts and Science. The views expressed in this article are those of the authors and do not necessarily reflect the official policy or position of the Air Force, the Department of Defense, or the United States Government.

REFERENCES

- ¹R. Ulbricht, E. Hendry, J. Shan, T. F. Heinz, and M. Bonn, *Reviews of Modern Physics* **83**, 543 (2011).
- ²Y.-S. Lee, *Principles of Terahertz Science and Technology* (Springer, New York, 2009).
- ³K. Vodopyanov, in *Solid-State Mid-Infrared Laser Sources*, *Topics in Applied Physics*, **89**, edited by I. Sorokina and K. Vodopyanov (Springer Berlin / Heidelberg, 2003) pp. 144–183.
- ⁴W. Shi, Y. J. Ding, and P. G. Schunemann, *Optics Communications* **233**, 183 (2004).
- ⁵K. Takeya, Y. Takemoto, I. Kawayama, H. Murakami, T. Matsukawa, M. Yoshimura, Y. Mori, and M. Tonouchi, *Europhysics Letters* **91**, 20004 (2010).
- ⁶K. Vodopyanov, *Laser & Photonics Reviews* **2**, 11 (2008).
- ⁷K. T. Zawilski, P. G. Schunemann, S. D. Setzler, and T. M. Pollak, *Journal of Crystal Growth* **310**, 1891 (2008).
- ⁸T. Wang, R. Sivakumar, D. Rai, W. Hsu, and C. Lan, *Journal of the Chinese Institute of Chemical Engineers* **39**, 385 (2008).
- ⁹M. H. Rakowsky, W. K. Kuhn, W. J. Lauderdale, L. E. Halliburton, G. J. Edwards, M. P. Sripsick, P. G. Schunemann, T. M. Pollak, M. C. Ohmer, and F. K. Hopkins, *Applied Physics Letters* **64**, 1615 (1994).
- ¹⁰T. Löffler, M. Kress, M. Thomson, T. Hahn, N. Hasegawa, and H. G. Roskos, *Semiconductor Science and Technology* **20**, S134 (2005).
- ¹¹I. Shoji, T. Kondo, A. Kitamoto, M. Shirane, and R. Ito, *Journal of the Optical Society*

of America B **14**, 2268 (1997).

¹²W. C. Hurlbut, Y.-S. Lee, K. L. Vodopyanov, P. S. Kuo, and M. M. Fejer, Optics Letters **32**, 668 (2007).

¹³V. Nathan, A. H. Guenther, and S. S. Mitra, Journal of the Optical Society of America B **2**, 294 (1985).

¹⁴F. Liu, Y. Li, Q. Xing, L. Chai, M. Hu, C. Wang, Y. Deng, Q. Sun, and C. Wang, Journal of Optics **12**, 095201 (2010).

¹⁵G. C. Bhar, Applied Optics **15**, 305 (1976).

¹⁶P. Kumbhakar, T. Kobayashi, and G. C. Bhar, Applied Optics **43**, 3324 (2004).

¹⁷M. Nagai, K. Tanaka, H. Ohtake, T. Bessho, T. Sugiura, T. Hirosumi, and M. Yoshida, Applied Physics Letters **85**, 3974 (2004).

¹⁸G. Q. Chang, C. J. Divin, C. H. Liu, S. L. Williamson, A. Galvanauskas, and T. B. Norris, Optics Express **14**, 7909 (2006).